Adaptive Techniques for Elastohydrodynamic Lubrication Solvers

C.E. Goodyer[a], R. Fairlie[a], M. Berzins[a] and L.E. Scales[b]*

[a]Computational PDEs Unit, School of Computing, University of Leeds, Leeds, LS2 9JT, United Kingdom

[b]Shell Global Solutions, Thornton, Chester, CH1 3SH, United Kingdom

The application of adaptive mesh techniques to the numerical solution of elastohydrodynamic lubrication calculations is described. Particular emphasis is placed on the use of variable timestep methods for transient problems. These methods are considered with reference to the differential algebraic formulation of the system to be solved. This approach is shown to be beneficial in reducing the computational work required. Finite difference grid adaptation is introduced and applied, with experimental results displaying the effectiveness of the methods.

1. Introduction

The solution of mathematical models of elastohydrodynamic lubrication (EHL) problems invariably requires the use of numerical methods. Industry demands fast and robust solvers for increasingly more complicated problems. The ability to reduce the work needed for individual problems is thus paramount. The mathematical and numerical analytic techniques behind many existing solvers combine traditional finite difference meshes with innovative multilevel methods. Numerical solutions have been computed since Petrusevich in 1951 [17], and finite difference, and to a lesser extent finite elements, have been used since then. The biggest advances have come from Lubrecht *et al.* with the application of multigrid in 1986 [13,14] and multilevel multi-integration in 1990 [4]. Modern techniques, such as wavelet preconditioning, have been tried [8] but it is unclear how well they will extend beyond the line contact case. Fixed regular grid, fixed timestep appears to be the standard way of solving EHL problems numerically.

Industry is now driving for solutions to more realistic - and hence more complicated - problems. This varies from transient cases, with variable loading and contact speeds, through complicated rheological behaviour, to solutions incorporating surface features and, ultimately, true roughness. This requires that the solvers being used must be designed to be extensible to meshes of several thousand points in each non-trivial direction, and, importantly, that the solutions can be obtained sufficiently quickly.

In many other application areas in which the rate of change of the solution does not remain constant with time, it has proved beneficial to vary the timestep to control the error in the solution [6]. The methods, thus, have obvious applications to EHL calculations. In Section 5 this will be examined, and speed-up results presented.

Early work was done by Lubrecht and coworkers [12,15] into the use of adaptive grids for EHL problems, however adaptive meshing and multigrid methods are not commonly combined. The ideas behind re-meshing are to be reexplored. It will be shown in Section 6 that without significantly changing the solution method, even just a two level adaptive mesh can achieve significant time savings. Choice of where to adapt is very important and preliminary results are presented based on solution based functions.

*The authors would like to thank EPSRC and Shell Global Solutions for funding this work through an EPSRC CASE Studentship for CEG. They also wish to thank the referees for their suggested improvements to this paper.

2. Notation

a	halfwidth of Hertzian contact
G	undeformed surface geometry
H	non-dimensionalised film thickness
H_{00}	film thickness central offset
K	film thickness kernel matrix
k	order of temporal method
m	iteration number
p_h	maximum Hertzian pressure
P	non-dimensionalised pressure
r	stepsize change ratio
R_x	reduced radius of curvature
T	non-dimensionalised time
u_s	sum of velocities of contacts
X	dimensionless coordinate
Y	dimensionless coordinate
z	viscosity index
α	pressure viscosity index
ϵ	coefficient in Reynolds equation
λ	coefficient in Reynolds equation
η_0	viscosity at ambient pressure
$\bar{\eta}$	non-dimensionalised viscosity
ρ	convergence test parameter
ρ_0	density at ambient pressure
$\bar{\rho}$	non-dimensionalised density

3. Equations and Standard Solution Method

The equations governing the EHL point contact are given, in non-dimensional form, by the following set of three equations. Firstly, the pressure distribution is defined by the discrete form of the Reynolds Equation:

$$\frac{\partial}{\partial X}\left(\epsilon\frac{\partial P}{\partial X}\right)+\frac{\partial}{\partial Y}\left(\epsilon\frac{\partial P}{\partial Y}\right)-\frac{u_s}{u_s(0)}\frac{\partial(\overline{\rho}H)}{\partial X}-\frac{\partial(\overline{\rho}H)}{\partial T}=0, \tag{1}$$

where ϵ and λ are given by

$$\epsilon=\frac{\overline{\rho}H^3}{\overline{\eta}\lambda u_s(0)}, \tag{2}$$

and

$$\lambda=\frac{6\,\eta_0\,R_x^2}{a^3\,p_h}. \tag{3}$$

The film thickness equation,

$$H(X,Y)=H_{00}+G(X,Y)+ \tag{4}$$

$$\frac{2}{\pi^2}\int_{-\infty}^{\infty}\int_{-\infty}^{\infty}\frac{P(X',Y')\,dX'\,dY'}{\sqrt{(X-X')^2+(Y-Y')^2}}, \tag{5}$$

defines the contact shape, for given undeformed geometry $G(X,Y)$.
The force balance equation,

$$\int_{-\infty}^{\infty}\int_{-\infty}^{\infty}P(X,Y)\,dX\,dY=\frac{2\,\pi}{3}, \tag{6}$$

is also solved to provide conservation of applied force.

Unless otherwise stated, the lubricant model used is that of a generalised Newtonian fluid. The model used for viscosity is derived from the Roelands equation [19],

$$\overline{\eta}(P)=exp\left\{\frac{\alpha\,p_0}{z}\left[-1+\left(1+\frac{Pp_h}{p_0}\right)^z\right]\right\} \tag{7}$$

and for density the Dowson and Higginson relation [7] is employed:

$$\overline{\rho}(P)=\left(1+\frac{5.8\times10^{-10}\,Pp_h}{1+1.7\times10^{-9}\,Pp_h}\right). \tag{8}$$

These equations are discretised on a regular (2^k+1) x (2^k+1) mesh. Both first and second order finite differences have been used. These have then been solved using the multigrid techniques described in [24,16,10] and the multilevel multi-integration algorithm of Brandt and Lubrecht [4].

4. DAE System

The EHL system defined by equations (1) to (8), once discretised, can be represented by a system of Differential-Algebraic Equations (DAEs) [6].

Defining the vector of film thicknesses across the whole domain, $\underline{H}$, and its multiple by the

function ρ in a pointwise manner by

$$\begin{array}{lll} [\underline{H}]_k = H_{i,j} & \text{for} & k = i + (j-1) \times N_x \\ \left[\underline{\rho H}\right]_k = \rho_{i,j} H_{i,j} & & i = 1, \ldots, N_x \\ & & j = 1, \ldots, N_y \end{array} \quad (9)$$

and the vector of pressures, $\underline{P}$, and densities, $\underline{\overline{\rho}}$, likewise, then the Reynolds Equation (1) is given by

$$\underline{F}_1(\underline{P}, \underline{\overline{\rho}H}) - \left[\underline{\overline{\rho}H}\right]' = 0, \quad (10)$$

and the film thickness equation, (4), by

$$\underline{F}_2(\underline{P}, \underline{H}) = 0, \quad (11)$$

where $'$ denotes differentiation in time. These can then be combined to define a DAE system for $\underline{U}^{\mathrm{T}} = (\underline{P}^{\mathrm{T}}, \underline{H}^{\mathrm{T}})$, by:

$$\underline{F}(\underline{U}, \underline{U}', t) = 0. \quad (12)$$

The solution method employed, described in [16] and [10], iteratively solves for pressure before updating the film thickness.

5. Variable Timesteps

For transient numerical calculations the choice of correct timestep size is critical. If the timestep is too large then important physical features may be missed should they fall between successive steps. Also, the calculated result may have larger local errors than are desirable for an accurate solution some timesteps later. Equally choosing a very small stepsize, may, at best, lead to a large amount of computational work for very small changes in the solution; at worse, result in solutions diverging, for example due to the magnification of temporal gradients. This is due, not to the stability of the problem, but the convergence properties of the non-linear solver outlined in Section 3 and described in detail in [9]. For example, in our experience should the timestep become very small then any corrections made may amplify, rather than reducing the errors in the solution unless very small underrelaxation parameters are used.

In EHL solutions ΔT has always been chosen to be fixed. Whilst for early transient solutions it was chosen to be larger than ΔX, the choice ΔT=ΔX has been pioneered by Venner and collaborators. This was introduced to minimise the total discretisation error for the Standard Upstream Second Order discretisation scheme which they employ. Wijnant [26] additionally proposed the use of ΔT=$2\Delta X$ for the Narrow Upstream Second Order scheme.

The optimal choice of timestep is governed by successfully relating the spatial error of the solution, with the time error. It is well established in the ODE literature, e.g. [1,22], that controlling the local (temporal) error per step, so that the spatial error dominates, provides efficient reliable algorithms. This approach, therefore, requires estimates of both components of the error.

Let the continuous equation system, defined by Equations (1) - (8), have an exact solution $\underline{u}(t)$, and the discretised equation system, defined by Equation (12), have exact solution $\underline{U}(t)$. If, at time t, the numerical approximation to the solution of the system is $\underline{\tilde{U}}(t)$, then the total error, $E(t)$, is defined by

$$\begin{aligned} \underline{E}(t) &= \underline{u}(t) - \underline{\tilde{U}}(t) \\ &= (\underline{u}(t) - \underline{U}(t)) + (\underline{U}(t) - \underline{\tilde{U}}(t)) \\ &= \underline{e}(t) + \underline{g}(t), \end{aligned} \quad (13)$$

where $\underline{e}(t) = \underline{u} - \underline{U}$ represents the spatial discretisation error, and $\underline{g}(t) = \underline{U} - \underline{\tilde{U}}$ is the global error in the time integration. Given that a solution has been discretised in space to a particular degree of accuracy, $\underline{e}(t)$, it is not worthwhile solving the transient part to a much higher degree of accuracy, but equally this transient error $\underline{g}(t)$ must not degrade the spatial accuracy.

The strategy we have employed is similar to that described in [6] for what is used in DASSL, which is designed to solve both index zero and index one DAE systems.

As outlined in Section 4, there is a free choice as to whether it is the errors in $\underline{P}$ or in $\underline{H}$ which are controlled. Intuitively, because the system given by (10) is solved for $\underline{P}$, and (11) is solved for $\underline{H}$ using this $\underline{P}$, it seems sensible to control the errors in $\underline{P}$. This was the approach suggested in [16]. However, it is the area inside the contact

region where the most change is taking place, and this is dominated by the wedge and squeeze terms in (1). This depends upon the film thickness, $\underline{H}$, which is also the algebraic variable of the system. Experiments have confirmed that controlling these errors requires significantly less work per timestep and less timesteps are required. The error tests will therefore be formulated for variable $\underline{H}$. However, note that if $\underline{P}$ is chosen instead, the only points to be considered for the error tests are non-cavitation ones.

Given that two different kinds of error need to be controlled, two different strategies need to be employed. First on an individual timestep, the code must to able to decide if the solution has converged far enough. To accomplish this, a strategy, such as the Shampine convergence test [21], must be used. In this test, the iteration cycle per timestep, m, is continued until

$$\frac{\rho}{1-\rho}\left\|\underline{H}^{(m+1)}(t_n)-\underline{H}^{(m)}(t_n)\right\| < 0.33tol, \quad (14)$$

where *tol* is an error tolerance for the iteration, $\|\cdot\|$ is a suitable norm (usually the root mean square), and ρ is defined by

$$\rho = \left(\frac{\left\|\underline{H}^{(m+1)}(t_n)-\underline{H}^{(m)}(t_n)\right\|}{\left\|\underline{H}^{(1)}(t_n)-\underline{H}^{(0)}(t_n)\right\|}\right)^{\frac{1}{m}}. \quad (15)$$

This cycle therefore relates the newly calculated solution, $\underline{H}^{(m+1)}(t_n)$ to that of the initially predicted solution $\underline{H}^{(0)}(t_n)$. To ensure that $\underline{H}^{(0)}(t_n)$ is a good prediction, linear interpolation of the pressure, film thickness and H_{00} are made from the previous two steps. This prediction typically brings the root mean square residual at the start of the timestep down by an order of magnitude.

Once this error test has been satisfied, a local error calculation is undertaken to establish a new timestep size. Since the EHL problem is a nonlinear DAE system, the LU decomposition of the system is not available, and hence the approaches described in [18] are not used. Instead, the local truncation error will be used to estimate the local error over the step. Defining the local truncation error for $\underline{P}$, $\underline{le\,P}$, as in [22, page 355], by:

$$\underline{le\,P} = \frac{1}{2}\left(P_n - P_n^{pred}\right), \quad (16)$$

and $\underline{le\,H}$ similarly, then the equations for these errors, in the same form as Equation (5.4.9) in [6], are

$$\begin{bmatrix} -1-\Delta T\frac{\partial \underline{F}_1}{\partial \overline{\rho} H} & -\Delta T\frac{\partial \underline{F}_1}{\partial \overline{\rho} P} \\ -\Delta T & \Delta T\,K \end{bmatrix} \begin{bmatrix} \underline{le\,H} \\ \underline{le\,P} \end{bmatrix} = \begin{bmatrix} -1 & 0 \\ 0 & 0 \end{bmatrix} \frac{1}{2} \begin{bmatrix} H_n - H_n^{pred} \\ P_n - P_n^{pred} \end{bmatrix}. \quad (17)$$

This gives us a relationship between the local truncation errors in $\underline{H}$ and $\underline{P}$:

$$\underline{le\,H} = K\,\underline{le\,P}, \quad (18)$$

where K is the film thickness integration kernel matrix. It is possible to rewrite the first equation of (17) as the standard estimate for the local truncation error:

$$-\Delta T\left(\frac{\underline{le\,H}}{\Delta T} + \frac{\partial \underline{F}_1}{\partial \overline{\rho} H}\underline{le\,H} + \frac{\partial \underline{F}_1}{\partial P}\underline{le\,P}\right) = -\frac{\left(\underline{H}_n - \underline{H}_n^{pred}\right)}{2}. \quad (19)$$

Since these Jacobians are never calculated, consider Taylor's Theorem for two variables:

$$\underline{F}_1\left(\overline{\rho}\underline{H} + \underline{le\,H}, \underline{P} + \underline{le\,P}\right) \approx \underline{F}_1\left(\overline{\rho}\underline{H}, \underline{P}\right) + \frac{\partial \underline{F}_1}{\partial \overline{\rho} H}\underline{le\,H} + \frac{\partial \underline{F}_1}{\partial P}\underline{le\,P} + h.o.t. \quad (20)$$

Assuming that the residual on the timestep, $\underline{F}_1\left(\overline{\rho}\underline{H} + \underline{le\,H}, \underline{P} + \underline{le\,P}\right)$ is zero, substitution into Equation (19) gives the following equation for the local errors $\underline{le\,H}$ and $\underline{le\,P}$:

$$\underline{F}_1\left(\underline{P}_n + \underline{le\,P}, \underline{\overline{\rho}H}_n + \underline{le\,H}\right) - \frac{\underline{\overline{\rho}H} + \underline{le\,H} - \underline{\overline{\rho}H}_n}{\Delta T} = \frac{1}{2\Delta T}\left(H_n - H_n^{pred}\right). \quad (21)$$

Defining $\underline{\tilde{P}} \equiv \underline{P}_n + \underline{le\,P}$ and $\underline{\tilde{H}}$ similarly, then the equation for the local error (21) may then be

rewritten in the same form as Equation (10) with a different right hand side:

$$\underline{F}_1\left(\underline{\tilde{P}},\underline{\overline{p}\tilde{H}}_n\right) - [\underline{\overline{p}\tilde{H}}_n]' = \frac{\left(H_n - H_n^{pred}\right)}{2\Delta T}. \qquad (22)$$

This equation may then be solved for $\underline{\tilde{H}}$ using the standard EHL multigrid algorithm with right hand side $\frac{1}{2\Delta T}\left(H_n - H_n^{pred}\right)$. Therefore, in summary, to estimate the local error on a timestep, after a sufficiently converged solution has been obtained, two or three more V-cycles are carried out to obtain solutions, $\underline{\tilde{P}}$ and $\underline{\tilde{H}}$, to the local error problem.

Once these new solutions are calculated, an estimate of the total local error in $\underline{H}$, may be defined as

$$\|\underline{le\,H}\|_\omega = \left\|\underline{\tilde{H}}_{n+1} - \underline{H}_{n+1}\right\|_\omega, \qquad (23)$$

where $\|\cdot\|_\omega$ is a weighted root mean square L_2-norm, as used in DASSL [6] defined by

$$\|\underline{H}\|_\omega = \sqrt{\frac{1}{N_x N_y}\sum_{i=1}^{N_x}\sum_{j=1}^{N_y}\left(\frac{H_{i,j}}{\omega_{i,j}}\right)^2}, \qquad (24)$$

with weights, $\omega_{i,j}$ defined by

$$\omega_{i,j} = ATOL + H_{i,j}^{(0)} RTOL \qquad (25)$$

which are themselves given in terms of the predicted solution at that mesh point, that timestep, $H_{i,j}^{(0)}$, and the absolute and relative error tolerances, $ATOL$ and $RTOL$ respectively. These tolerances have been chosen to be dynamically defined by

$$ATOL = \frac{1}{10}\sqrt{\frac{1}{N_x^C N_y^C}\sum_{I=1}^{N_x^C}\sum_{J=1}^{N_y^C}\left[\tilde{H}_{i,j} - \tilde{H}_{I,J}\right]^2} \qquad (26)$$

and

$$RTOL = ATOL, \qquad (27)$$

for fine mesh points (i,j) with coincident coarse points (I,J).

Once the local error has been established, it is then necessary to use this information to calculate the most desirable stepsize for the next timestep. The method chosen here is that of Shampine and Gordon [23], where any change to the step size is governed by the value of r in

$$r = (2\|\underline{le\,H}\|_\omega)^{\frac{-1}{k+1}}, \qquad (28)$$

with k being the order of the method ($k = 1$ for the Backward Euler Method). The method of [23] suggests that the new stepsize should be given by

$$\Delta T_{n+1} = r\Delta T_n, \qquad (29)$$

subject to some limitations.

These tests now mean that the code itself relates future timestep sizes to the magnitude of the local error. If the error is small, e.g. $r > 1.5$ in Equation (28), then the stepsize may be increased for the next timestep. If the error is 'too large', $r < 0.9$, then the stepsize is reduced, either for the following step, or, if the current step is considered to have failed, the current timestep may be retaken with a new stepsize. There is also a 'comfort region' in between these extremes where the stepsize is left unchanged.

Limits are also imposed on when, and by how much the timestep size may change. In some codes, as is used here, it is never allowed to change up or down by more than a factor of 2. This helps, both in terms of keeping temporal derivatives of similar scales, and in keeping a check on what changes are allowed. A safety factor - usually of just one timestep - prevents the stepsize increasing too rapidly. The size is, however, allowed to reduce as often as necessary to capture features in the solution. Maximum and minimum timesteps may be specified by the user before runtime. These allow controls to be placed on the code to stop the stepsize diminishing towards nothing, for example, if it is failing at some point, and to impose physical constraints to the individual problem being solved: e.g. if we were on T=[0.0s, 1.0s] then there would be no point in a ΔT_{max} of 0.5s, but 0.05s could be acceptable.

5.1. Examples

A clear example of the benefits of using variable timesteps can be seen in the case of reversal of entrainment. This test case is that used

Parameter	Value
Viscosity index	2.1×10^{-8} Pa^{-1}
Maximum Hertzian pressure	0.45GPa
Material parameter, G	2961
Load parameter, W	6.58×10^{8}
Speed parameter, U	1.47×10^{9}
Moes parameter, M	52.2
Moes parameter, L	6.9

Table 1
Non-dimensionalised parameters for reversal example

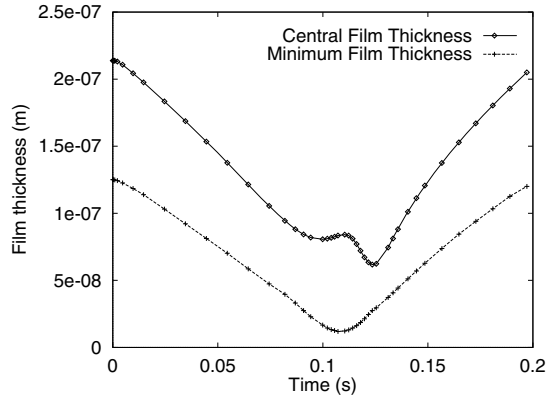

Figure 1. Central and minimum film thicknesses for reversal of entrainment

in [20] and shows oil entrainment being linearly decreased from $0.05ms^{-1}$ to $-0.05ms^{-1}$ in 0.2s. The most interesting - and nonlinear - part of this example is the saucer of viscous fluid that forms at the point of reversal (0.1s) and proceeds across the domain (towards the new outflow) before the deformation pattern re-adopts its characteristic horseshoe shape. All physical parameters are as given in [20], with the non-dimensionalised quantities as given in Table 1.

Figure 1 shows the central and minimum film thicknesses during this example. The points on the line indicate where timesteps have been taken.

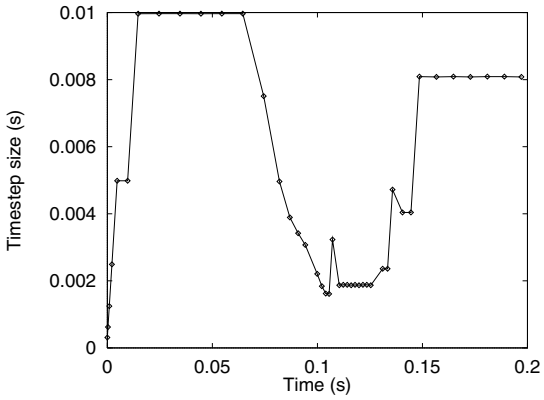

Figure 2. Timestep sizes for reversal of entrainment

It can be seen that these are clustered around reversal and just after, as was desired. The actual timestep sizes can be seen in Figure 2 and the values of r, the stepsize change ratio, can be seen in Figure 3.

It was explained above that there can be advantages in not changing the stepsize too often. Choosing the new stepsize based on an *a priori* error test cannot guarantee that the new stepsize will be valid for more than one timestep. Thus having the range of values for r in Equation (28) where the stepsize remains unchanged is important. The size of this region also governs how often the step size can change because if it is too small then the stepsize may be successively increased and decreased. This 'chattering' effect, well known in the ODE community, may cause instabilities in the solution. This region is considered, for example, by Shampine [23] and Hairer *et al.* [11]. It is the range of values calculated for r in the error test, for which r should be set to 1 in Equation (29).

The use of variable timestepping may require more iterations to reach the same level of approximation for the solution at individual timesteps. However, the important factor is not that more cycles may be needed per timestep, but that these

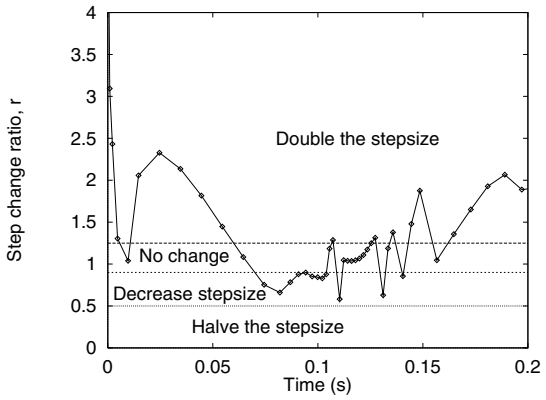

Figure 3. Stepsize change ratio, r, values for reversal of entrainment example

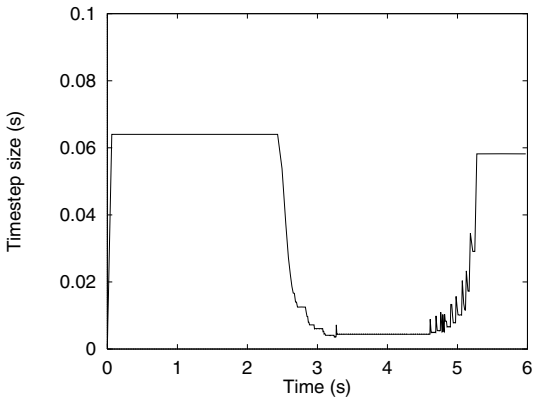

Figure 4. Timestep size during overrolling of a transverse ridge

are being done considerably less often. It is also possible to limit the number of iterations per timestep if the convergence of individual steps is failing to satisfy the convergence test (14) quickly enough.

The local error test is an additional overhead per timestep and this does involve several multigrid cycles, hence in cases where a stepsize is unlikely to change, less frequent checking is required. A good example of this is the overrolling of a transverse ridge, (after Venner and Lubrecht [25]) where the ridge entered the domain outside the area of influence on the solution, before progressing through. The stepsizes taken for this case are shown in Figure 4 where a large timestep is suitable before and after the period when the ridge is in the contact area, but a small stepsize is desirable in between.

One of the stated aims for the use of variable time stepping, was a reduction in the required computational time. Returning to the reversal example of earlier, Table 2 shows the computational time comparison between run times for fixed step ($\Delta T = \Delta X$) and variable timestep sizes. To confirm the validity of the results obtained, central and minimum film thicknesses are compared in Table 3 at two reference times:

Grid Dimension	Fixed / Variable	Time taken (s)	Iterations required
65×65	Fixed	7909	9558
65×65	Variable	3192	3387
129×129	Fixed	79151	11367
129×129	Variable	35142	5145

Table 2
Computational performance comparison between fixed and variable timestepping codes

Film thickness $\times 10^{-8}$ m		t=0.1 s		t=t_{min}≈0.108 s	
		Minimum FT	Central FT	Minimum FT	Central FT
65×65	Fixed	1.592	7.871	1.061	8.153
65×65	Variable	1.659	8.069	1.200	8.356
129×129	Fixed	2.146	7.975	1.664	8.339
129×129	Variable	2.216	8.136	1.744	8.509

Table 3
Film thickness (FT) comparisons at two reference times between fixed and variable timestepping codes

the point of reversal (t=0.1 s) and the time that the minimum film thickness is achieved (t=t_{min}≈0.108 s). At these times the minimum film thickness is an order of magnitude less than the initial steady state. It is clear that the significant saving in computational work described, produces results of similar accuracy.

6. Grid Adaptation

The addition of more fine grid points means that the resolution of the solution can be increased. However, it may not be necessary to use a fine grid in regions where the solution does not change greatly. The intention of adaptive meshing is to focus the computational work by placing mesh points in the areas of the domain where they are required.

Solutions of the EHL system are characterised by three regions of the domain: the contact region, where the pressure is high; the non-contact region, where the pressure is low; and the cavitation region, where the pressure is assumed to be identically zero. In the contact region, a fine mesh is used for both film thickness and deformation calculations, whereas inside the cavitation region an adapted mesh is used for film thickness, but the Reynolds Equation is not solved. An adpted mesh may be applied in the remainder of the domain.

In cases where solution discontinuities or very steep gradients exist, the solution at these points must be updated differently from smooth parts of the solution, otherwise smearing of the numerical discontinuity will not allow accurate resolution of physical features. These ideas were used by Harten to produce a multilevel approximation strategy, called multiresolution (see [2] for 2D work). In this work, the single fine grid is stored only at nodes which are needed to interpolate the calculated solution in order to obtain the solution at the rest of the mesh, using smoothness properties. This reduces both the computational work required in evaluating the new solution, and the storage of said solution.

It is straightforward to extend Harten's work to multigrid. Multigrid grid adaptation has been undertaken for many years, e.g. [3], including some work with EHL solvers [12,15]. Here the problem is being re-examined to use adaptive techniques to generate a full fine grid representation of the solutions. Hence, the adaptive mesh multilevel multi-integration techniques described in [5] will not be required, although this will be an obvious extension to this work.

In the EHL multilevel solver, even with multi-integration, the largest proportion of the time is spent in calculating the deformation on the finest grid. Away from the contact region, pressures are locally small and hence the deformations are too. At such a point, assuming the deformation in the region around it to be smooth, it may be interpolated from suitable nearby points. Provided that any oscillations in the deformation (for example, due to surface roughness) are adequately resolved on this coarser mesh, then this approximation is valid.

The film thickness deformation solve may be the largest computational expense of the calculation, but as the mesh size increases, so does the linear algebra system that requires solving for the pressure. Reducing the number of points used in these calculations can make even further

Grid Dimensions	Regular grid run time (s)	Adapted grid run time (s)
65×65	5	3
129×129	61	50
257×257	878	669
513×513	13568	9732

Table 4
Computational performance comparison between fixed and adaptive mesh codes for 5 V(3,1) cycles

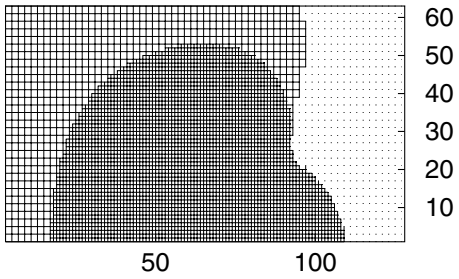

Figure 5. Example of an adapted mesh

improvements to code performance. Again, especially away from the contact region, and always in the interior of the cavitation region, there is little point in the unnecessary calculation of a smooth solution.

The hierarchical structure for multigrid is defined with successive refinements of the mesh. Adaptation require careful consideration of the re-discretisation of the equations from Section 3 to ensure that only 'valid' information is being used. This is especially important on the boundary between regions of different levels of refinement. There are also issues which need to be carefully considered with respect to the coarsening and prolonging in the refined regions: for example, if the whole fine grid was de-refined one level, then the coarse grid correction process should reflect that this adapted grid and the next coarsest are the same computational domain.

The experiments we have performed so far have been restricted to one level of de-refinement on the finest mesh, plus the cavitation region. Experimental results of timings, as shown in Table 4, are very encouraging. They show the speed-up between unadapted and adapted grids over 5 multigrid V(3,1) cycles. The domain has been refined similar to Figure 5 where the adaptation has been guided by the solution. On the finest mesh regions with $P < 0.001$ have all been refined for both pressure and film thickness calculations. In the cavitation region, where Equation (1) is not valid, the pressure has not been solved, and the film thickness has been calculated on the adapted grid.

The extension of this approach to a fully automatic apdaptation algorithm will require suitably accurate error estimates. It will also include the possibility for mesh de-refinement where appropriate.

7. Conclusions and Future Work

Two methods for improving the computational efficiency of multigrid finite difference EHL codes have been presented. Variable timestepping has been shown, by experiments, to substantially reduce the required work whilst maintaining the same level of solution accuracy. The overhead in calculating new stepsizes is small, relative to the increase in performance. Changing the stepsize away from ΔT, within predefined limits, has been seen to pose no problems for the solver.

Adaptive meshing has been introduced and early results have shown it to be successful in reducing the computation time of the calculation on the finest mesh. Although it has been restricted here to just the finest grid level, it is clear that extending the same ideas up through the multigrid structure will produce even greater benefits. Further work on a fully adaptive mesh, with more than two levels of refinement on the same grid, is the next progression. These adaptive meshing techniques must then be further extended to become more automatic, focussing the computa-

tional effort where it is needed most. Further computational speed up may be achieved through the use of parallelisation of the code [9].

REFERENCES

1. M. Berzins. Temporal error control for convection-dominated equations in two space dimensions. *SIAM Journal of Scientific Computation*, 16(3):558–580, 1995.
2. B. L. Bihari and A. Harten. Multiresolution schemes for the numerical solution of 2-D conservation laws I. *SIAM Journal on Scientific Computing*, 18(2):315–354, 1997.
3. A. Brandt and C. W. Cryer. Local mesh refinement multigrid techniques. *SIAM Journal on Scientific and Statistical Computing*, 8(2):109–134, 1987.
4. A. Brandt and A. A. Lubrecht. Multilevel matrix multiplication and fast solution of integral equations. *Journal of Computational Physics*, 90(2):348–370, 1990.
5. A. Brandt and C. H. Venner. Multilevel evaluation of integral transforms on adaptive grids. Technical Report WI/GC-5, Weizmann Institute of Science, 1996.
6. K. E. Brenan, S. L. Campbell, and L. R. Petzold. *Numerical Solution of Initial-Value problems in Differential-Algebraic Equations.* SIAM, 1996.
7. D. Dowson and G. R. Higginson. *Elastohydrodynamic Lubrication, The Fundamentals of Roller and Gear Lubrication.* Permagon Press, Oxford, Great Britain, 1966.
8. J. Ford, K. Chen, and L. E. Scales. A new wavelet transform preconditioner for iterative solution of elastohydrodynamic lubrication problems. Report, Chester College, England, 1999.
9. C. E. Goodyer. *Adaptive Numerical Methods for Elastohydrodynamic Lubrication.* PhD thesis, University of Leeds, Leeds, England, in preparation.
10. C. E. Goodyer, R. Fairlie, M. Berzins, and L. E. Scales. An in-depth investigation of the multigrid approach for steady and transient EHL problems. In D. Dowson and M. Priest, editors, *Thinning films and Tribological Interfaces, Proceedings of the 26th Leeds-Lyon Symposium on Tribology.* Elsevier, 2000.
11. E. Hairer, S. P. Nørsett, and G. Wanner. *Solving Ordinary Differential Equations I: Nonstiff Problems.* Springer-Verlag, 1980.
12. A. A. Lubrecht. *Numerical solution of the EHL line and point contact problem using multigrid techniques.* PhD thesis, University of Twente, Endschende, The Netherlands, 1987.
13. A. A. Lubrecht, W. E. ten Napel, and R. Bosma. Multigrid, an alternative method of calculating film thicknesses and pressure profiles in elastohydrodynamically lubricated line contacts. *Trans. ASME, Journal of Tribology*, 108(4):551–556, 1986.
14. A. A. Lubrecht, W. E. ten Napel, and R. Bosma. Multigrid, an alternative method of solution for two-dimensional elastohydrodynamically lubricated point contact calculations. *Trans. ASME, Journal of Tribology*, 109:437–443, 1987.
15. A. A. Lubrecht, C. H. Venner, W. E. ten Napel, and R. Bosma. Film thickness calculations in elastohydrodynamically lubricated circular contacts, using a multigrid method. *Trans. ASME, Journal of Tribology*, 110:503–507, 1988.
16. E. Nurgat. *Numerical Methods in Lubrication Modelling.* PhD thesis, University of Leeds, Leeds, England, 1997.
17. A. I. Petrusevich. Fundamental conclusions from the contact-hydrodynamic theory of lubrication. *Izv. Akad. Nauk. SSSR (OTN)*, 2:209, 1951.
18. L. Petzold. Differential/algebraic equations are not ode's. *SIAM Journal of Scientific and Statistical Computation*, 3(3):367–384, 1982.
19. C. J. A. Roelands. *Correlational Aspects of the viscosity-temperature-pressure relationship of lubricating oils.* PhD thesis, Technische Hogeschool Delft, The Netherlands, 1966.
20. L. E. Scales, J. E. Rycroft, N. R. Horswill, and B. P. Williamson. Simulation and observation

of transient effects in elastohydrodynamic lubrication, SP-1182. In *SAE International Fuels and Lubricants Meeting, Dearborn, Michigan*, pages 23–34, 1996.

21. L. F. Shampine. Implementation of implicit formulas for the solution of ODEs. *SIAM Journal of Scientific and Statistical Computation*, 1(1):103–118, 1980.
22. L. F. Shampine. *Numerical Solution of Ordinary Differential Equations.* Chapman and Hall, 1994.
23. L. F. Shampine and M. K. Gordon. *Computer Solution of Ordinary Differential Equations : the Initial Value Problem.* W. H. Freeman and Co., 1975.
24. C. H. Venner. *Multilevel Solution of the EHL Line and Point Contact Problems.* PhD thesis, University of Twente, Endschende, The Netherlands, 1991.
25. C. H. Venner and A. A. Lubrecht. Numerical simulation of a transverse ridge in a circular EHL contact under rolling/sliding. *Trans. ASME, Journal of Tribology*, 116:751–761, 1994.
26. Y. Wijnant. *Contact Dynamics in the Field of Elastohydrodynamic Lubrication.* PhD thesis, University of Twente, Endschende, The Netherlands, 1998.